Journal of Sustainable Engineering & Renewable Energy (JSERE)

VOLUME 1 ISSUE 2 (2025)

PUBLISHED BY
E-PALLI PUBLISHERS, DELAWARE, USA

Journal of Sustainable Engineering & Renewable Energy (JSERE)

Volume 1 Issue 2, Year 2025
ISSN: 3069-9215 (Online)
DOI: https://doi.org/10.54536/jsere.v1i2.5930
https://journals.e-palli.com/home/index.php/jsere

CFD-Driven Optimization of Intake Manifold Design for Enhanced Volumetric Efficiency and Performance in Formula SAE Internal Combustion Engines

Swift N. K. Onyegirim[1*], Ifeanyichukwu U. Onyenanu[1], Kennedy C. Owuama[1], Philip N. Atanmo[1]

Article Information

Received: April 02, 2025

Accepted: May 07, 2025

Published: December 29, 2025

Keywords

Airflow Optimization, Computational Fluid Dynamics (CFD), Design Optimization, Engine Performance, Formula SAE, Intake Manifold, Internal Combustion Engine, Steady-State Analysis, Turbulence Modeling, Volumetric Efficiency

ABSTRACT

This study investigates the optimization of an internal combustion engine (ICE) intake manifold through the application of Computational Fluid Dynamics (CFD) analysis, aiming to enhance volumetric efficiency and overall engine performance, particularly within the context of Formula SAE applications. The research employs steady-state CFD simulations to rigorously assess airflow dynamics, pressure distribution, and turbulence characteristics across a variety of intake runner configurations. Critical design parameters, including runner length, plenum volume, and restrictor geometry, are meticulously analyzed to mitigate cylinder-to-cylinder variation and maximize airflow uniformity. The findings reveal that optimized intake manifold geometries, including straight-runner designs, can enhance turbulent kinetic energy by as much as 11% while concurrently diminishing flow disparities among cylinders. Supersonic flow conditions (Mach > 1) are detected in proximity to critical sections, thereby underscoring the necessity for precise geometric tuning to alleviate compressibility effects. The selection of materials, specifically Glass Fiber Reinforced Plastic (GFRP), is substantiated based on its thermal and structural appropriateness. This study emphasizes the effectiveness of CFD-driven design methodologies in reducing development costs and timeframes, all while facilitating performance enhancements. Future research endeavors should incorporate transient CFD models and experimental validation to further optimize dynamic engine performance in authentic racing scenarios.

INTRODUCTION

Due to the requirement for increased efficiency, lower emissions, and better power output, computational fluid dynamics (CFD) analysis of intake manifold systems has been a crucial area of research in recent years for the design and optimization of internal combustion engine (ICE) performance. To ensure consistent distribution of the air-fuel mixture, which has a direct impact on volumetric efficiency, combustion stability, and overall engine performance, the intake manifold is essential. (Halis & Kocakulak, 2024; Rajkumar *et al.,* 2018). Intake manifold geometry optimization using traditional experimental techniques is frequently expensive and time-consuming, involving dynamometer testing and intensive prototyping. CFD simulations, on the other hand, offer a practical and economical substitute, allowing for a thorough examination of the intake system's fluid dynamics, turbulence, and pressure distribution before actual production (Halis & Kocakulak, 2024; Verma, 2017). Adaptive mesh refinement (AMR), high-fidelity turbulence models, and transient boundary conditions that take valve timing effects into account have all been included in recent CFD tool developments like ANSYS Fluent, CONVERGE, and STAR-CCM+, which have greatly increased simulation accuracy. (Ahsan & Noman, 2024; Rajkumar *et al.,* 2018).

In multi-cylinder engines, where geometric asymmetries can result in cylinder-to-cylinder differences in air-fuel ratios, combustion efficiency, and emissions, one of the main issues in intake manifold design is providing uniform airflow distribution over all cylinders. (Shin *et al.,* 2022). Volumetric efficiency and engine output may be greatly affected by relatively little changes in runner length, plenum volume, or cross-sectional area, according to studies. When curved and straight intake manifolds were compared, for example, it was discovered that straight designs improved combustion stability by reducing cylinder-to-cylinder variance by 1.1% and increasing turbulent kinetic energy around top dead center (TDC) by up to 11% (Shin *et al.,* 2022). Furthermore, the implementation of variable-length intake manifolds (VLIM) has demonstrated potential in maximizing resonance effects across a range of engine speeds; within particular operating ranges, some configurations have enhanced volumetric efficiency by 6.33% and thermal efficiency by 1.77% (Shin *et al.,* 2022). The evaluation of innovative intake manifold shapes, such as helical or tumble-enhancing ports, which encourage in-cylinder swirl and tumble movements essential for effective air-fuel mixing and flame propagation, has also benefited greatly from CFD analysis. (Ahsan & Noman, 2024; Cecere *et al.,* 2023). Numerical simulations of hydrogen-direct injection (H2DI) engines, for instance, demonstrate how crucial intake port design is to minimizing aberrant combustion (such as backfire) and optimizing power density through the use of thermal management and turbocharging techniques. (Goyal *et al.,* 2024). Additionally, lightweight materials like magnesium and aluminum alloys are being used more often in manifold designs to increase thermal efficiency and decrease inertial losses; CFD simulations

[1] Department of Mechanical Engineering, Chukwuemeka Odumegwu Ojukwu University, Uli, Nigeria
[*] Corresponding author's e-mail: sk.onyegirim@coou.edu.ng

have confirmed that these materials are structurally sound under high-pressure and temperature circumstances. (Halis & Kocakulak, 2024; Souza *et al.,* 2019).

The development of high-performance intake systems has been further advanced by the combination of CFD with optimization methods like Taguchi design of experiments (DoE) and Response Surface Methodology (Ukachi *et al.,* 2024). These techniques greatly cut down on development time and expenses by allowing engineers to determine ideal design parameters like runner diameter, plenum shape, and diffuser angles with few testing runs (Rajkumar *et al.,* 2018; Verma, 2017). The use of machine learning methods to improve CFD predictions has also been investigated recently, allowing for the real-time optimization of intake manifold shapes under dynamic operating circumstances (Ahsan & Noman, 2024). Even with these developments, it is still difficult to adequately describe transient flow phenomena such as pulsing airflow during valve opening and closing and interactions with exhaust gas recirculation (EGR) or turbocharger systems (Cecere *et al.,* 2023; Nikolaev *et al.,* 2025). The creation of multi-physics CFD models that integrate fluid dynamics with structural and thermal evaluations, as well as the investigation of additive manufacturing methods for creating intricate, topology-optimized manifold designs, which are examples of future research objectives (Souza *et al.,* 2019; Thamaraikanan *et al.,* 2015). The use of CFD in the design of next-generation intake manifolds will grow as global emissions standards tighten, guaranteeing that ICEs will continue to be competitive in a future of electrification and sustainable fuels. (Goyal *et al.,* 2024; Shin *et al.,* 2022).

LITERATURE REVIEW

Through Computational Fluid Dynamics (CFD) analysis of intake manifold systems, the reviewed body of research provides a strong argumentative basis for combustion engine design and performance optimization. Each study discusses and improves on various aspects of intake geometry, thermodynamic performance, and combustion behavior. Although they acknowledge performance trade-offs at high speeds, Luo *et al.* (2016) contend that improving intake manifold geometry with spacers and chamber width improves airflow uniformity and fuel efficiency under a range of engine speeds. In response, Bondar *et al.* (2020) advocated for a mathematical optimization of runner length using Helmholtz resonance theory, which may hypothetically boost airflow and volumetric efficiency without the need for internal adjustments like spacers. Shin *et al.* (2022) bolster the argument for geometry-led performance tweaking by demonstrating that straight manifolds increase in-cylinder turbulence and decrease cylinder-to-cylinder variance. Liang *et al.* (2025), on the other hand, move the discussion to cold-start behavior and suggest a new burner system in the intake to enhance preheating through CFD-optimized spray atomization. They contend that operational factors such as airflow velocity control combustion efficiency, particularly in extremely cold temperatures. While introducing a dynamic, variable-length manifold model optimized through genetic algorithms, Talati *et al.* (2022) uphold the notion of geometry-driven optimization and provide better efficiency metrics than static solutions. Regarding racing applications, Barhm Mohamad *et al.* (2020) and Niti Kammuang-lue and Borikhut (2015) Support simulation-led design with AVL-Boost and experimental verification, respectively, showing that customized intake configurations in Formula Student cars improve torque and lower pressure drops. The integration of these multi-domain results (combustion, geometry, cold-start, and acoustics) into a single, high-resolution CFD model that can be used for both road and performance engines under varying operating circumstances is still lacking, though. When considered collectively, these studies show that CFD analysis allows for accurate intake manifold optimization, but they also highlight a substantial knowledge gap about how to combine these particular design components into a comprehensive system that can dynamically adjust to changing engine operating conditions. This is necessary to create an intake manifold system that is truly optimized for any internal combustion engine application.

MATERIALS AND METHODS

Design pathway

The flowchart in Figure 1 shows how to use CFD and experimental techniques to optimize an internal combustion engine's intake manifold systematically. To guarantee durability and heat resistance from the design requirement, material selection comes after design criteria, which establish performance goals and restrictions. The geometric and functional characteristics are defined by the technical standards and description, and they are then converted into a CAD drawing for manufacture and

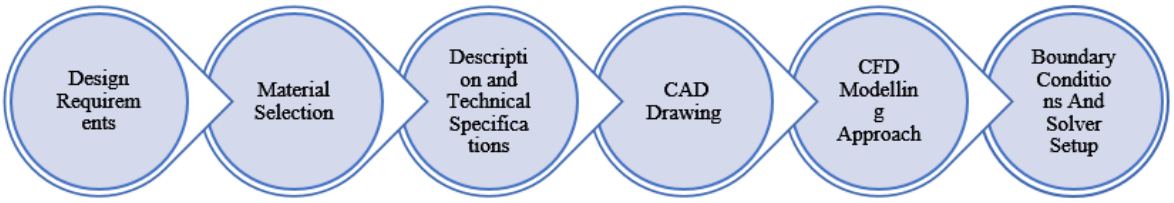

Figure 1: Design Fabrication Pathway

simulation (Ezechukwu *et al.*, 2025). Mesh, turbulence modeling, and flow analysis are all part of the CFD modeling process. For accurate simulation, boundary conditions (Ezechukwu *et al.,* 2025; Jugu *et al.,* 2025) and solver setup specify temperature, inlet/outlet pressures, and solver parameters.

Design Requirement and FSAE Intake Manifold

Given that the FSAE intake manifold serves as an air buffer to control airflow to the cylinders, its design is essential to maintaining steady engine performance. The intake manifold, which is shaped by available space and the best pickup point to prevent heat and aerodynamic disruptions, is responsible for distributing air uniformly throughout the cylinders in normally aspirated engines. Triangular side-fed log manifolds are typically preferred in FSAE applications because of their ability to balance packing and performance. Another important factor is the manifold's size; it should ideally be double the engine capacity to supply ample air volume without delaying throttle response. A precisely designed convergent-divergent nozzle is necessary to reduce pressure losses and enhance volumetric efficiency since the FSAE-mandated 20 mm intake restrictor severely restricts airflow. For air control, the throttle body, which is placed before the restrictor, is essential. Despite some flow blockage, the butterfly valve is frequently chosen for its dependability and simplicity. Intake runners further increase performance through tailored lengths that use acoustic wave behavior to maximize volumetric efficiency via air ramming. To guarantee high performance and responsive engine behavior in an FSAE race car, these elements must be optimized in tandem through simulation and design iterations.

Material selection

Material selection is an essential part of every design and, as such, is given utmost priority to prevent breakdown or part failure. Having seen that these three materials are mainly the materials used in the manufacture of the intake manifold, it is therefore paramount that the best of these materials is utilized.

The following properties are considered for the material selection of the intake manifold: operating temperature, pressure, weight loss/density, cost effectiveness, and formability; hence, these materials.

- Polyethylene (PE)
- Glass fiber reinforced plastic (GFRP)
- Polypropylene (PP)

Glass fiber reinforced plastic (GFRP) was decided to be used because of its great thermal properties and the low weight/density compared with other stated materials above.

Table 1: Properties of the considered material selection

S/N	Materials	Properties			
		Thermal conductivity (W/m ^{0}C)	**Specific Heat (J/ Kg ^{0}C)**	**Thermal Expansion Coefficient (µstrain/ ^{0}C)**	**Density (Kg/m^3)**
1.	GFRP	0.55	1.2	33	1.97 E^3
2.	Polypropylene (PP)	0.167	1.96 E^3	180	910 E^3
3.	Polyethylene (PE)	0.435	1.88 E^3	198	960 E^3

Description and Specification

Table 2: Engine specification of Honda CBR600RR

S/N	Description	Values
1.	**Manufacture/model**	**2006 Honda CBR600RR**
2.	Bore /stroke/cylinders/displacement	67.00/42.50mm (2.6 x 1.7 inches)/4 cylinder/ 599cc
3.	Cooling	Liquid
4.	Valves/Valves per cylinder/Valve configuration	16/4/DOHC
5.	Compression ratio	12.0:1.00
6.	Induction	
7.	Fuel type	Gas - Normal 98 octane unleaded petrol
8.	Max power design RPM	86KW/13,000min-1 (95/1/EC)
9.	Max Torque design RPM	86Nm/11,000min-1 (95/1/EC)
10.	Min RPM for 80% max torque	7500rpm
11.	Fuel system (manf'r)	Student designed/ built a tank & PGM-DSFI electronic fuel injection
12.	Fuel system sensor position and crank position	Air temp. /Coolant temp./ throttle

13.	Fuel Pressure	3.5 bar (static)
14.	Injector Location	70mm/3.1 inches
15.	Intake Plenum Volume	2400cc cylindrical body
16.	Effective intake Runner Length	Approximately 210mm/8.2 inches
17.	Exhaust Header design	4-2-1 equal length
18.	Effective Exhaust runner Length	520mm/ 20.4 inches header
19.	Ignition System	Computer-controlled digital transistorized with electronic advance.
20.	Ignition Timing	Independent 4-Cylinder 3D-Mapped Computer control.
21.	Spark Plug Type	IMR9C-9H (NGK); VUH27D (ND)
22.	Battery Capacity	12V/8.6AH
23.	Oiling System (wet/dry sump, mods)	Honda forced pressure and wet sump
24.	Coolant System and Radiator Location	Single radiator mounted in the side pod
25.	Fuel Tank Location, type	Mounted on chassis over Engine – Aluminum sheet tank
26.	Muffler	High performance carbon fiber muffler for CBR600 (Laser)

Type of Engine: On a Formula-SAE race car, the rules restrict the usage of engine types to being

- a reciprocating piston-type engine;
- utilizing a four-stroke combustion cycle;
- of a displacement not exceeding 610cc.

In addition to the restrictions on the engine, it is required that an engine operating on gasoline as a fuel type must have an air intake restrictor through which all of the air entering the engine must pass. On the intake manifold system, the restrictor is placed between the throttle mechanism and the engine itself. It must also not be movable or flexible in any way. This restrictor is circular and limited to 20mm in diameter. Limitations to air intake dimensions are introduced as a bid to limit the overall power of the engine, and subsequently the vehicle, to reduce the speeds of the built vehicles on the track. It also adds an element of design variation as an off-the-shelf engine cannot be directly used on the car, spurring students to have to design a suitable air intake system to reduce the impact of the air restrictor on the entire engine system. The engine selected for the Ugo FSAE racing Car is the Honda CBR 600RR (Ukwu *et al.,* 2016; Onyenanu *et al.,* 2015). It is the most practical option to meet the driving conditions and FSAE requirements.

CAD Modeling Details

The geometric model of the intake system was created, and a mesh was generated using SOLIDWORKS 2023 software. Computational fluid dynamics analysis was achieved in CFD software.

Figure 2: 3D Model of Intake Manifold for 2006 HONDA CBR 600RR

The model design would resemble the path of air entering the Intake Manifold and through the runners and into the engine cylinders. The model was meshed with meshing software. The flow simulation was performed by using the CFD software, the simulations were run based on the Navier–Stokes equations under the K–ε Two-equation turbulent model at steady state. The air density was assumed to be constant in the simulation, as shown in Tables 5 & 6 are the variations and boundary conditions in each of the CFD simulations conducted in the present work. The simulation setting is based on the modeled intake manifold with a runner length of 305mm, and

thus, the CFD and experimental results can be compared. Similarly, the setting is maintained in all the intake runners of the manifold.

Size of Computational Domain

Table 3: Size of Computational Domain

X min	-0.155 m
X max	0.240 m
Y min	-0.269 m
Y max	0.035 m
Z min	-0.162 m
Z max	0.101 m

Meshing details

The entire discretization of the geometry for numerical analysis is indicated by the 44,283 total cells in the analysis mesh for the computational model. The areas where fluid movement takes place, like within the intake manifold passageways, are represented by 13,980 fluid cells. The solid components, such as the manifold walls or other structural elements involved in heat conduction or mechanical contact, are represented by 17,050 solid cells. There are also 13,253 partial cells, which provide precise boundary representation and usually show up at the interfaces of complicated geometries or fluid-solid zones.

Table 4: Basic Mesh Dimensions

Number of cells in X	22
Number of cells in Y	18
Number of cells in Z	16

Boundary Conditions and Their Calculation

Table 5: Boundary Conditions parameters

Type	**Environment Pressure**
Faces	Face<1>@Boss-Extrude7
Coordinate system	Face Coordinate System
Reference axis	X
Thermodynamic parameters	Environment pressure: 101325.00 Pa Temperature: 293.20 K
Turbulence parameters	Turbulence intensity and length Intensity: 2.00 % Length: 0.003 m
Boundary layer parameters	Boundary layer type: Turbulent

Static Pressure 1

Table 6: Static pressure parameters

Type	**Static Pressure**
Faces	Face<5>@LID1
Coordinate system	Face Coordinate System
Reference axis	X
Thermodynamic parameters	Static pressure: 96080.00 Pa Temperature: 293.20 K
Turbulence parameters	Turbulence intensity and length Intensity: 2.00 % Length: 0.003 m
Boundary layer parameters	Boundary layer type: Laminar

The constant pressure boundary conditions were used to define the fluid pressure at the inlet and outlet of the air intake system. The inlet pressure was considered as 1.013 bar (101325.00 Pa) since the flow was assumed to take place at WOT (Wide Open Throttle). For outlet runners, cylinder pressures of 0.9 bar (96080.00 Pa) were considered, since the normal expected range of cylinder pressure in the SI engine at intake stroke is 0.7 to 1.2 bar. The turbulence specification method used for this study was of 'Intensity and Hydraulic Diameter'. Hydraulic diameter and turbulent intensity calculations were done using the engine parameters, shown in Table 7 below.

Table 7: Engine parameter

Bore diameter (D)	67 mm (0.067m)
Stroke length (L)	42.5 mm (0.0425)
Engine rpm (N)	7500 (125rev/sec)
Inlet Diameter (restrictor)	20 mm (0.020)
Inlet area (A)	314.2 mm^2 (3.142×10^-4 m^2)

From the above engine parameters, the swept volume for the engine can be calculated as follows, which was used to determine the velocity of air at the inlet port.

$$Q = \frac{\pi}{4} \times D^2 \times L \times N \times \frac{x}{n}$$

$Q = 3.142/4 \times 0.067^2 \times 0.0425 \times 125 \times 4/2$

$= 0.7855 \times 0.00449 \times 0.0425 \times 250$

$= 0.0375\ m^3/s$

Where x is the number of cylinders taken as 4 and n = 2 for 4-stroke engines.

$$V = {}^{Q}/_{A}$$

$$V = {}^{0.0375}/_{0.0003142}$$

$= 119.265\ m/s$

Where, V is velocity of air at the inlet port.

Thus, Velocity of air at Inlet Port=119.265 m/sec. Since the runner outlets are directly connected to the inlet port of the cylinder head, the velocity at the inlet ports is assumed as the velocity at the runner outlets

Performance Metrics

Volumetric Efficiency

Volumetric Efficiency is a measure of the Cylinder Charge. It defines the amount of fresh charge that can be sucked into the cylinder, as a ratio of the theoretical mass of air that will be contained in the cylinder (Pszczólkowski, 2022). Essentially, for a normally aspirated gasoline engine, it is the ratio of the trapped volume of gas to the volume of the cylinder.

Volumetric Efficiency, $\gamma_a = \frac{m_g}{m_{th}} = \frac{m_g}{V_H \cdot \rho_{th}} = \frac{V_G}{V_H}$

$m_g = V_g . \rho_g = the$ Mass of air that is trapped in the cylinder

$m_{th=}$ Theoretical mass of air that can be trapped in the cylinder

$V_H = V_{th}$ = Volume of the cylinder, which equals theoretical Volume

$V_{g=}$ Volume of gas trapped in the cylinder

Assumptions

Theoretical density of air in the cylinder, ϱ_{th} = Density of ambient air, ϱ_g

The Cylinder Charge of an engine determines the amount of power that can be produced, and varies with air-fuel ratios as well as RPM. At the exact stoichiometric ratio, the power produced is proportional to the mass of air (or air-fuel mixture) being supplied to the engine, otherwise known as the "charge" of the engine. In the scenario where the only method of charging the engine is by the vacuum pressure created by the expansion of the combustion chamber when the piston falls, it can achieve a maximum volumetric efficiency of 100%(Pszczólkowski, 2022; Xu, 2020).

Choked flow

The phenomenon of a choked flow system is one about compressible flow, such as that of air in the atmospheric environment flowing through the air intake system, and into the engine's cylinders. In the FSAE context, the main location in which choked flow is likely to develop would be at the air intake restrictor. It is formed when air flows across a path with a decreasing cross-sectional area (Sawant *et al.,* n.d.; Wable & Shah, 2017). The mass flow rate under a choked flow condition would be defined by the following formula:

$$\dot{m} = CA\sqrt{k\rho\left(\frac{2}{k+1}\right)\frac{k+1}{k-1}}; kg/s \text{ (Shelagowski \& Mahank, 2015)}$$

c = discharge coefficient, A = discharge joule cross-sectional area, m^2, K = C_p/C_v of the gas, C_p = specific heat of the gas at constant pressure, C_v = specific heat of the gas at constant volume, ϱ= real gas density at P and T, kg/m^3, P = absolute upstream pressure of gas, Pa.

To complete the calculations, the various values of the air's properties need to be plugged into the formula. Certain assumptions are made about the condition of the air, such as its composition, as air is a mixture of various types of gases. The exact value would have slight differences, but should generally be in the same range of values. The calculation below shows the values used:

C=1, A=3.142*10-4m^2 (20mm diameter restrictor), C_p = 29.19 J/mol.K, C_v = 20.85 J/mol.K, k = 1.4, ϱ = 1,2041 kg/m^3, P = 101325Pa

$$\text{mass flow rate, } \dot{m} = CA\sqrt{k\rho\left(\frac{2}{k+1}\right)\frac{k+1}{k-1}} = 0.075 kg/s$$

$$\text{Volume flow rate} = 0.0624 m^3/s$$

In this calculation, a discharge coefficient of 1 is taken, though the number is typically smaller than this. The discharge coefficient is the ratio of the actual flow rate to the ideal flow rate of the gas, given the same initial (before restriction) conditions. The calculations therefore provide the ideal mass flow rate, and the result is taken as a reference maximum.

Considering David Vizard's Rule for IM Runner Length;

The general rule is that you should begin with a runner length of 17.8 cm for a 10,000-rpm peak torque location, from the intake opening to the plenum chamber. You add 4.3 cm to the runner length for every 1000 rpm that you want the peak torque to occur before the 10,000 rpm.

Therefore, the desired peak torque should occur at 6,000 rpm the total runner length should be

17.8 cm + (4 x 4.3 cm) = 35.0 cm.

The effective intake runner diameter is given by;

D = SQRT (N x displacement x VE)/3330

D = Intake runner diameter (in inches), SQRT = Square root, N = Target RPM for peak torque = 6000rpm, Displacement (in liters) = 599cc = 0.599litres, VE = Volumetric efficiency in %

But VE is represented by this formula;

VE = Vg/Vh,

Where, Vg = Volume of gas trapped in a cylinder

Vg = Total displacement volume of engine/No. of cylinder

Vg = 599/4 = 149.75cc

Vh = Volume of Cylinder, which equals the theoretical volume

Vh = (Vg/CR) + Vg; CR (Compression ratio of engine, 12.0:1.0)

Vh = (149.75/12.0) + 149.75 = 12.479 + 149.75 = 162.229cc

: · VE = 149.75/162.229 = 0.92 = 92%

D = SQRT (6000 x 0.599 x 0.92)/3330

D = 2.992inches = 75.997mm

Hence, the effective intake runner diameter is 75.997mm

The plenum volume for high RPM at peak torque and power output is in the range of 1.3 to 1.5 times to cylinder volume. Taking the ratio of 1.3

Therefore, plenum volume = 0.599 x 1.3

Intake Plenum volume now becomes 0.7787litres (778.7cc = 778700mm^3)

Calculations of the Ram intake tube.

The inside diameter of a Ram intake tube is given by;

D = SQRT {(Displacement x VE x Redline)/ (V x 18.5)}
Where, Redline = RPM at maximum power = 7500rpm
V = Velocity of air flow in the intake manifold plenum for resonance, usually estimated at 180ft/sec. maximum.
D = SQRT {(0.599 x 0.92 x 7500)/ (180 x 18.5)}
D = 1.241inches = 31.526mm =32mm
Hence, the diameter of the Ram intake tube is 32mm
Length of the Ram (Plenum elbow) Intake Tube;
The length of a Ram tube with peak torque at 6000 rpm is 13 inches. For higher or lower RPM, 1.7 inches is added to 13 inches for every 1000 rpm subtracted from 6000 rpm, whereas 1.7 inches is subtracted from 13 inches for every 1000 rpm added to 6000 rpm.
The RPM at Redline = 7500 rpm
Hence, 7500 – 6000 = 1500
1500/1000 = 1.5
1.5 x 1.7 = 2.55inches
Length of Ram intake tube = 13inches – 2.55inches = 10.45inches
Therefore, length of Ram intake tube = 10.451inches = 265.43mm = 265mm

RESULTS AND DISCUSSION

Results of the CFD Analysis

The steady-state analysis has been carried out for five different conditions

1. All runners open.
2. 1st runner open.
3. 2nd runner open.
4. 3rd runner open
5. 4th runner open

Analysis Goals for Runners; 1,2,3 & 4

Four intake runners in a fluid dynamic system are thoroughly analyzed using the performance data from Tables 8 and 9, which assess flow parameters including temperature, density, velocity, and pressure. The bulk average velocities, mass flow rates, and intake and exit pressures are almost equal for every runner, indicating steady flow behavior and system balance. Average static pressure (~96132 Pa), bulk average velocity (~20.2 m/s), and inlet mass flow rate (~0.0596 kg/s) are almost the same for Runners 1, 2, and 4, but Runner 3 has slightly higher static pressure (96762 Pa) and mass flow (~0.0623 kg/s), suggesting a slightly higher throughput. Although they are not utilized in convergence, maximum velocities are continuously higher than 500 m/s. Mach numbers peak at 1.51, indicating supersonic flow conditions in isolated locations, whereas temperature data for all runners vary from 271.82 K to about 398.85 K. Shear stress and vorticity measurements show considerable shear and turbulence close to surfaces, and density varies from 0.32

Table 8: Goals Datum for Intake Runners 1, 2, 3, and 4

Name	Unit	Use in convergence	Runner 1				Runner 2				Runner 3				Runner 4			
			Value	Progress	Delta	Criteria	Value	Progress	Delta	Criteria	Value	Progress	Delta	Criteria	Value	Progress	Delta	Criteria
GG Av Static Pressure	Pa	On	96132.22	14	1358.25	192.14	96131.89	14	1400.16	193.94	96762.17	12	1539.84	180.70	96132.22	14	1358.25	192.14
GG Bulk Av Velocity	m/s	On	20.21	5	18.87	1.00	19.06	5	18.00	0.95	18.88	5	16.54	0.85	20.21	5	18.87	1.00
Maximum Velocity	m/s	Off	515.72	1e-08	294.22	14.88	515.76	1e-08	294.14	14.88	496.82	1e-08	280.99	14.38	515.72	1e-08	294.22	14.88
SG Av Static Pressure (at Inlet)	Pa	On	34845.23	5	40650.61	1994.37	34841.20	5	40647.31	1994.49	38603.54	5	38591.09	1881.60	34845.23	5	40650.61	1994.37

Mass Flow Rate (at Outlet)	SG Bulk Av Total Pressure (at Outlet)	SG Av Static Pressure (at Outlet)	SG Av Density (at Inlet)	SG Bulk Av Velocity (at Inlet)	Mass Flow Rate (at Inlet)	SG Bulk Av Total Pressure (at Inlet)
kg/s	Pa	Pa	kg/m³	m/s	kg/s	Pa
On	On	On	Off	Off	On	On
1e-08	96442.85	96442.85	0.42	459.99	0.06	101325.00
1000	1000	13	1e-08	1e-08	6	100
1e-08	1539.70	1539.70	0.40	263.71	0.05	5.82e-11
1e-08	192.96	192.96	0.02	13.76	0.00	0.00
1e-08	96408.24	96408.24	0.42	460.02	0.06	101325.00
1000	1000	13	1e-08	1e-08	6	100
1e-08	1543.43	1543.43	0.40	263.64	0.05	5.82e-11
1e-08	193.68	193.68	0.02	13.76	0.00	0.00
-0.06	97326.34	96080.00	0.47	433.42	0.06	101325.00
6	6	100	1e-08	1e-08	6	100
0.06	1861.05	0.00	0.38	251.25	0.05	5.82e-11
0.00	108.52	1.63	0.02	12.95	0.00	0.00
1e-08	96442.85	96442.85	0.42	459.99	0.06	101325.00
1000	1000	13	1e-08	1e-08	6	100
1e-08	1539.70	1539.70	0.40	263.71	0.05	5.82e-11
1e-08	192.96	192.96	0.02	13.76	0.00	0.00

to 1.16 kg/m³. When taken as a whole, the data shows that each intake runner exhibits steady, although complicated, aerodynamic behavior, with Runner 3 showing somewhat more flow and temperature uncertainty.

Global Min-Max-Table Runners; 1,2,3 & 4

Table 9: Runner 1, 2, 3, and 4 Datum

Name	Unit	Min	Max	Min	Max	Min	Max	Min	Max
		Runner 1		Runner 2		Runner 3		Runner 4	
Pressure	Pa	27733.24	98762.36	27728.08	98704.85	30065.28	98775.08	27733.24	98762.36

Temperature	K	285.14	398 Pillars of Creation	398.81	285.14	398.85	271.82	392.99	285.14
Density (Fluid)	kg/ m3	0.33	1.15	0.32	1.15	0.35	1.16	0.33	1.15
Velocity	m/s	0	529.936	0	529.966	0	500.432	0	529.936
Velocity (X)	m/s	-84.233	34.059	-84.885	35.462	-83.402	33.208	-84.233	34.059
Velocity (Y)	m/s	-65.204	486.704	-64.661	486.731	-74.592	430.261	-65.204	486.704
Velocity (Z)	m/s	-55.920	280.129	-56.140	280.147	-59.047	267.196	-55.920	280.129
Temperature (Fluid)	K	285.14	398.81	285.14	398.85	271.82	392.99	285.14	398.81
Mach Number	-	0	1.51	0	1.51	0	1.45	0	1.51
Vorticity	1/s	1.931e-04	38470.836	4.935e-04	37222.837	9.591e-004	43116.647	1.931e-04	38470.836
Shear Stress	Pa	0	192.58	0	191.65	0	186.30	0	192.58
Relative Pressure	Pa	-73591.76	-2562.64	-73596.92	-2620.15	-71259.72	-2549.92	-73591.76	-2562.64
Heat Transfer Coefficient	W/ m2/K	0	0	0	0	0	0	0	0
Surface Heat Flux	W/ m2	0	0	0	0	0	0	0	0

Velocity Contours

When air moves from the plenum intake to Runner 1, the simulation indicates a considerable decrease in velocity because the increased plenum area diffuses the flow.

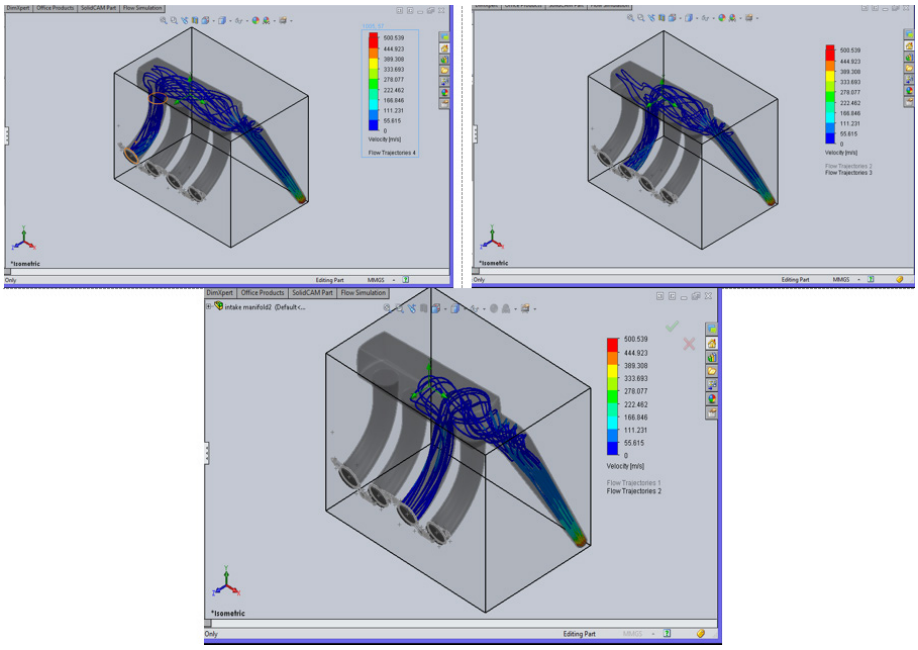

Figure 3: Contours of velocity magnitude for runners 1, 2, and 3

Smooth flow entrance is disrupted by a steep curve at the plenum-runner junction. Because of a less abrupt geometric transition from the plenum, runner 2 has a smoother flow entrance at its intake, as seen by its greater velocity. According to this section, Runner 2's local region saw an increase in velocity, indicating velocities that were more in line with the usual runner velocity of the CBR600RR (~100–130 m/s at 13,000 RPM). At its intake, runner 3 has high velocity, suggesting effective plenum flow entrance.

Contours of Static Pressure

Figure 6 shows static pressure contours for Runner 1 when only Runner 1 is open, indicating a sudden velocity drop from the plenum inlet to the runner, correlated with a pressure increase due to flow stagnation at the plenum's end corners. Static pressure in Runner 1's inlet is likely in the range of 105,000-115,000 Pa, based on a prior CBR600RR estimate of ~110,000 Pa. The sharp bend at Runner 1's inlet likely causes localized pressure losses, reducing efficiency. Runner 2's pressure is higher compared to all-runners-open conditions, reflecting reduced flow demand and stagnation effects in the plenum. Pressure regions form at the plenum's end corners, with Runner 2's inlet likely experiencing pressures around 110,000–120,000 Pa. Runner 3 exhibits elevated pressure (~110,000–120,000 Pa) due to stagnation in the plenum and focused flow through a single runner. This section indicates that pressure is higher in single-runner conditions compared to all runners open, where pressure drops due to distributed flow.

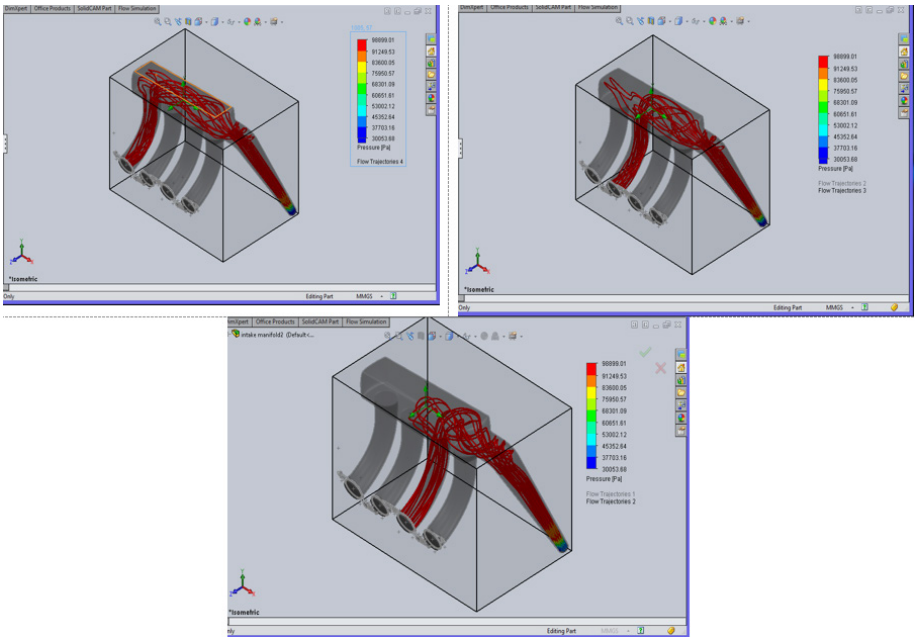

Figure 4: Contours of static pressure magnitude for runners 1, 2, and 3

Mach number

Supersonic flow is indicated by the Mach number of 1.51, and Runners 1 and 2 exhibit notable compressibility effects, resulting in a 47% change in density. As a result, downstream pressure drops and engine duty rises. The CBR600RR's high-performance intake is shown by the steep curve in restricted spaces, which exacerbates flow acceleration. The smoother intake shape of runner 2 enables efficient flow acceleration, increasing the Mach values of the restrictor. Both downstream pressure and engine performance are impacted by the drastic density loss (47% at supersonic flows). The high Mach number of runner 4 is probably the result of a shortened restrictor and an efficient intake design, which raises engine effort because of the density drop and lower downstream pressure.

The computational fluid dynamics (CFD) study of an intake manifold is summarized in Table 16, with particular attention to important flow characteristics among its runners. Airflow along each channel is steady and fast, as seen by the velocity across runners 1 through 3, which ranges from a minimum of 55.615 m/s to a maximum of 500.539 m/s. Effective pressure recovery and distribution are suggested by the pressure distribution in runners 1 through 3, which ranges from 30,052.68 Pa to 98,899.01 Pa. With isolated supersonic portions (Mach > 1), probably close to important sections of the geometry, the Mach number, which represents the ratio of flow speed to the speed of sound, ranges from 0 to 1.45 in all runners (including runner 4). This information demonstrates consistent flow characteristics for every runner and validates how well the intake manifold design controls compressible, high-speed airflow.

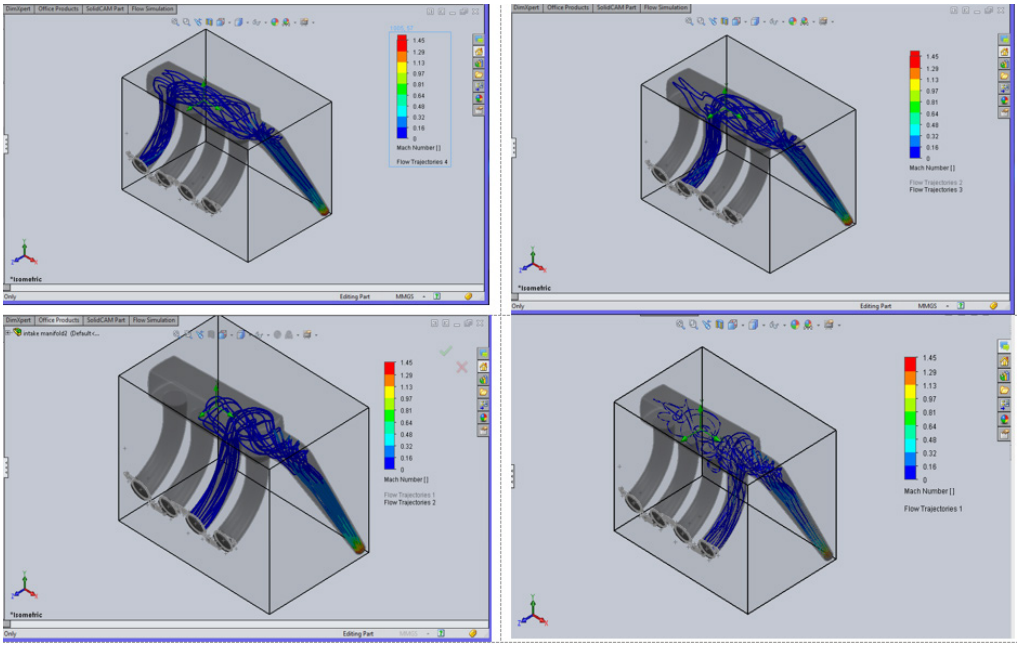

Figure 5: Contours of Mach number magnitude for runners 1, 2, 3, and 4

Table 10: Summary of the analysis

Analysis	Min	Max
Velocity (m/s) runner 1	55.615	500.539
Velocity (m/s) runner 2	55.615	500.539
Velocity (m/s) runner 3	55.615	500.539
Pressure (pa) runner 1	30052.68	98899.01
Pressure (pa) runner 2	30052.68	98899.01
Pressure (pa) runner 3	30052.68	98899.01
Mach for runner 1	0	1.45
Mach for runner 2	0	1.45
Mach for runner 3	0	1.45
Mach for runner 4	0	1.45

CONCLUSION

The CFD-based optimization of the intake manifold for the 2006 Honda CBR600RR engine has yielded significant insights into improving volumetric efficiency and airflow uniformity. The study confirms that geometric modifications, such as straight-runner configurations and optimized plenum volumes, enhance turbulent kinetic energy and reduce cylinder-to-cylinder variation, directly benefiting engine performance. The presence of localized supersonic flow (Mach 1.51) near the restrictor underscores the importance of aerodynamic refinement to mitigate density losses and pressure drops. Material analysis supports the use of GFRP for its lightweight and thermal resilience, aligning with high-performance requirements. While steady-state simulations provide a robust foundation, future research should prioritize transient CFD models to capture dynamic engine behaviours, such as throttle response and RPM fluctuations. Experimental validation through dynamometer testing is recommended to bridge simulation-application gaps. This work advances intake manifold design methodologies, offering scalable solutions for both racing and commercial ICE applications, and highlights the potential of integrating machine learning for real-time optimization in evolving engine technologies.

Recommendations

Future studies should concentrate on using transient CFD models to capture dynamic engine characteristics, such as fluctuating RPM and throttle inputs, which are crucial for FSAE racing performance, to improve the intake manifold design's dependability and application. It is advised to validate CFD results experimentally by testing prototypes on a dynamometer to evaluate performance in real-world racing scenarios. Investigating sophisticated turbulence models, such as Large Eddy Simulation (LES), may increase the precision of flow forecasts in intricate geometries. To guarantee long-term dependability, durability testing of GFRP under vibrational stress is also recommended. The construction

of high-performance intake manifolds that maximize volumetric efficiency and power output while abiding by FSAE limits is made possible by these recommendations, which are important because they close the gap between simulation and real-world application. By providing a scalable framework for intake system optimization across a range of internal combustion engine applications, from racing to commercial cars, this study advances CFD-driven design approaches.

REFERENCES

Ahsan, M., & Noman, M. (2024). Improving Internal Combustion Engine Performance through Inlet Valve Geometry and Spray Angle Optimization: Computational Fluid Dynamics Study. *Engineering Proceedings, 72*(1), 6. https://doi.org/10.3390/engproc2024072006

Bondar, V., Aliukov, S., Malozemov, A., & Das, A. (2020). Mathematical model of thermodynamic processes in the intake manifold of a diesel engine with fuel and water injection. *Energies, 13*(17), 4315. https://doi.org/10.3390/en13174315

Cecere, G., Irimescu, A., & Merola, S. S. (2023). Design of an Optically Accessible Intake Manifold for Characterization of Liquid and Gaseous Jets in PFI Operating Conditions. *Designs, 7*(1), 24. https://doi.org/10.3390/designs7010024

Ezechukwu, V. C., Braide, T. K., Onyenanu, I. U., Ayadinuno, G., Agwaziam, J. O., & Ojinekeya, C. O. (2025). Structural Simulation Analysis of the Developed Hybrid of Aluminum Composites and Carbon Nanotube Brake Disc. *International Journal of Applied and Natural Sciences, 3*(1), 18–28. https://doi.org/10.61424/ijans.v3i1.195

Ezechukwu, V. C., Onyenanu, I. U., Ayadinuno, G., & Agwaziam, J. O. (2025). Structural simulation analysis of the developed hybrid of Momordica angustisepala fiber and Breadfruit seed-shell particles composites, Bolted Flanges. *IPS Journal of Engineering and Technology, 1*(1), 13–20. https://doi.org/10.54117/ijet.v1i1.2

Goyal, H., Jones, P., Bajwa, A., Parsons, D., Akehurst, S., Davy, M. H., Leach, F. CP., & Esposito, S. (2024). Design trends and challenges in hydrogen direct injection (H2DI) internal combustion engines – A review. *International Journal of Hydrogen Energy, 86*, 1179–1194. https://doi.org/10.1016/j.ijhydene.2024.08.284

Halis, S., & Kocakulak, T. (2024). RSM-based optimization of lambda and mixed fuel concentration parameters of an LTC mode engine. *Energy, 306*. 132550. https://doi.org/10.1016/j.energy.2024.132550

Jugu, E. B., Onyenanu, I. U., & Nwobi-Okoye, C. C. (2025). Finite Element Analysis and Factorial Optimization of Heat Treatment Flaws in CNG Pressure Vessels: Implications for Structural Integrity and Safety. *Scientific Journal of Engineering, and Technology, 2*(1), Article 1. https://doi.org/10.69739/sjet.v2i1.487

Kammuang-lue, N., & Borikhut, W. (2015). Development of intake manifold for Student Formula CMU F-914 using theoretical and simulated designs. *Food Agricultural Sciences and Technology, 1*(2), 39–45. retrieved from https://ph02.tci-thaijo.org/index.php/stej/article/view/251356

Liang, T., Liu, J., Mo, H., Lee, C., Wang, Z., Li, Z., & Cong, M. (2025). Effects of operating conditions on flame evolution and preheating performance of intake manifold burner aided by spray atomization. *International Journal of Heat and Fluid Flow, 112*, 109730. https://doi.org/10.1016/j.ijheatfluidflow.2024.109730

Luo, F., Wang, C., Xue, F., Ye, B., & Wu, X. (2016). A Study on the Influence of Fuel Pipe on Fuel Injection Characteristics of Each Nozzle Hole in Diesel Injector. *MATEC Web of Conferences, 40*, 02016. https://doi.org/10.1051/matecconf/20164002016

Mohamad, B., Karoly, J., & Zelentsov, A. (2020). CFD modelling of formula student car intake system. *Facta Universitatis, Series: Mechanical Engineering, 18*(1), 153-163. https://doi.org/10.22190/FUME190509032M

Nikolaev, V. K., Skvortsov, A. A., Khudayarov, Z. F., & Nikolaev, R. S. (2025). Optimization of the exhaust catalytic manifold of an internal combustion engine. *Journal of Materials Science: Materials in Engineering, 20*(1), 30. https://doi.org/10.1186/s40712-025-00238-3

Onyenanu, I. U., Swift, O. N. K., & Atanmo, P. N. (2015). Design and Analysis of a Tubular Space Frame Chassis for FSAE Application. *International Journal of Emerging Technologies and Innovative Research (JETIR), 2*(10), 134-140. http://www.jetir.org/papers/JETIR1510025.pdf

Pszczólkowski, J. (2022). The model for cylinder charge parameters during engine starting. *Combustion Engines, 188*(1), 60–66. https://doi.org/10.19206/CE-142029

Ragupathi, P., Rajkumar, S., & Hussain, R. S. (2014). Design and analysis of diesel engine intake manifold using CFD simulation. *International Journal of Modern Trends in Engineering and Science, 1*(1), 174-179. https://www.researchgate.net/publication/323393337_Design_and_Analysis_of_Diesel_Engine_Intake_Manifold_using_CFD_Simulation

Sawant, S. S., Gurav, P. N., Nivalkar, P. S., Sawant, P. M., & Waghmare, D. S. N. (2018). Design And Fabrication of Air Intake for FSAE Race Car. *IJSART, 4*(2).

Shelagowski, M., & Mahank, T. (2015). CFR Formula SAE intake restrictor design and performance. In *Proceedings of the 2015-ASEE North Central Section Conference American Society for Engineering Education.* https://asee-ncs.org/wp-content/uploads/2021/12/proceedings/2015/Paper%20files/Student_Papers/2015_ASEE_NCS_Conference_submission_29.pdf

Shin, K., Son, S., Moon, J., Jo, Y., Kwon, J. S.-I., & Hwang, S. (2022). Dynamic modeling and predictive control of boil-off gas generation during LNG loading. *Computers & Chemical Engineering, 160*, 107698. https://doi.org/10.1016/j.compchemeng.2022.107698

Souza, G. R. de, Pellegrini, C. de C., Ferreira, S. L., Soto Pau, F., & Armas, O. (2019). Study of intake

manifolds of an internal combustion engine: A new geometry based on experimental results and numerical simulations. *Thermal Science and Engineering Progress, 9*, 248–258. https://doi.org/10.1016/j.tsep.2018.12.003

Talati, H., Aliakbari, K., Ebrahimi-Moghadam, A., Khoshbakht Farokhad, H., & Eskandary Nasrabad, A. (2022). Optimal design and analysis of a novel variable-length intake manifold on a four-cylinder gasoline engine. *Applied Thermal Engineering, 200*, 117631. https://doi.org/10.1016/j.applthermaleng.2021.117631

Thamaraikanan, R., Anish, M., Kanimozhi, B., George, T., & Koshy, V. G. (2015). Design and Analysis of an Intake Manifold in an IC Engine. *Applied Mechanics and Materials,* 766–767, 1021–1027. https://doi.org/10.4028/www.scientific.net/AMM.766-767.1021

Ukachi, P., Okonkwo, U. C., & Onyenanu, I. U. (2024). Appraisal of the Insulation Potential of Rice Husk Ash Reinforced Calabash-Epoxy Composite for Vehicle Firewall Application. *International Journal of Engineering Research, 13*(08). https://doi.org/10.17577/IJERTV13IS080018

Ukwu, N. O., Onyenanu, I. U., & Atanmo, P. N. (2016). Design and Analysis of FSAE Brake System using locally sourced Material", *International Journal of Emerging Technologies and Innovative Research (JETIR), 3*(2), 82-89, Available: http://www.jetir.org/papers/JETIR1602018.pdf

Verma, M. K., Verma, D., & Shukla, A. Design & Optimization of Intake Manifold of Carburetor Using Computational Fluid Dynamics. *Momentum, 11*, 0. https://www.academia.edu/114160321/design_and_optimization_of_intake_manifold_of_carburetor_using_computational_fluid_dynamics

Wable, P. V., & Shah, S. S. (2017). Air flow optimization of venturi type intake restrictor. *International Journal of Engineering Development and Research, 5*(4), 483-489. https://rjwave.org/ijedr/viewpaperforall.php?paper=IJEDR1704075

Xu, R. (2020). The Relationship between Volume & Pressure and Rotation & Torque in an Engine Cylinder. *Saudi Journal of Engineering and Technology, 5*(11), 484–485. https://doi.org/10.36348/sjet.2020.v05i11.015